Discovery of ω-free high-temperature Ti-Ta-*X* shape memory alloys from first-principles calculations

Alberto Ferrari [1,*] Alexander Paulsen,[2] Dennis Langenkämper,[2] David Piorunek,[2] Christoph Somsen,[2] Jan Frenzel,[2] Jutta Rogal,[1,†] Gunther Eggeler,[2] and Ralf Drautz[1]

[1]*Interdisciplinary Centre for Advanced Materials Simulation, Ruhr-Universität Bochum, 44801 Bochum, Germany*
[2]*Institut für Werkstoffe, Ruhr-Universität Bochum, 44801 Bochum, Germany*

The rapid degradation of the functional properties of many Ti-based alloys is due to the precipitation of the ω phase. In the conventional high-temperature shape memory alloy Ti-Ta, the formation of this phase compromises completely the shape memory effect, and high ($>100\,°$C) transformation temperatures cannot be maintained during cycling. A solution to this problem is the addition of other elements to form Ti-Ta-*X* alloys, which often modifies the transformation temperatures; due to the largely unexplored space of possible compositions, very few elements are known to stabilize the shape memory effect without decreasing the transformation temperatures below $100\,°$C. In this study, we use transparent descriptors derived from first-principles calculations to search for new ternary Ti-Ta-*X* alloys that combine stability and high temperatures. We suggest four alloys with these properties, namely Ti-Ta-Sb, Ti-Ta-Bi, Ti-Ta-In, and Ti-Ta-Sc. Our predictions for the most promising of these alloys, Ti-Ta-Sc, are subsequently fully validated by experimental investigations, the alloy Ti-Ta-Sc showing no traces of ω phase after cycling. Our computational strategy is transferable to other materials and may contribute to suppress ω phase formation in a large class of alloys.

I. INTRODUCTION

Among the first discovered smart materials, shape memory alloys (SMAs) [1–9] are attractive at present for actuating applications, efficient energy conversion, and flexible medical instruments and implants. SMAs are ferroelastic materials characterized by a thermal memory, the so-called one-way effect (1WE): If deformed at low temperature, SMAs are able to recover a predetermined shape by heating.

The 1WE is based on a reversible, solid-to-solid martensitic phase transformation between the high-temperature phase (austenite) and the low-temperature phase (martensite): Heating an SMA from low temperature induces the nucleation and growth of austenite at the austenite start temperature A_s, and, *vice versa*, cooling an SMA from high temperature induces the nucleation and growth of martensite at the martensite start temperature M_s.

The vast majority of the engineering applications of SMAs use Ni-Ti [10,11] as base material because it combines a durable and reversible 1WE with exceptional physical and mechanical properties. However, the transformation temperatures A_s and M_s of this SMA are lower than $100\,°$C [12,13], which limits the opportunities for designing smart material components in hot environments.

A possible alternative to Ni-Ti as high-temperature shape memory alloys (HTSMAs) [14,15] are Ti-Ta alloys [16–32]. In these alloys, the transformation temperatures A_s and M_s increase with decreasing Ta concentration c_{Ta}, and they can

be as high as $430\,°$C when c_{Ta} is reduced to 20 at. % [30]. The 1WE in Ti-Ta is due to a martensitic transformation between the austenitic phase β, a solid solution of Ti and Ta with a body-centered-cubic lattice and spacegroup $Im\bar{3}m$, and the martensitic phase α'', with an orthorhombic lattice and spacegroup *Cmcm*.

Unfortunately, at Ta concentrations where the transformation temperature is higher than $100\,°$C ($c_{Ta} < 33$ at. %) the 1WE in Ti-Ta is not stable and the shape recovery strain decreases rapidly to zero after only a few thermal cycles. The functional degradation of the 1WE in Ti-Ta, as in other β-Ti alloys [33], is caused by nano-precipitation of the ω phase [20,21,23–25,34], a detrimental phase with a hexagonal lattice and spacegroup $P6/mmm$. The microstructural, thermodynamic, and kinetic aspects of the formation of the ω phase have recently been discussed in terms of a time-temperature-transformation diagram for Ti-Ta [35]. The rate of nucleation of the ω phase is observed to be lower at higher c_{Ta}, but the formation of this phase in Ti-Ta cannot be avoided unless c_{Ta} is increased until A_s and M_s become lower than $100\,°$C, a regime in which Ni-Ti is usually preferred for engineering applications. Other detrimental phases (α and α') [36] are observed only at very low c_{Ta}.

It has been observed in experiments [21–23,37] that alloying Al, Sn, or Zr in moderate ($\leqslant 5$ at. %) concentrations to Ti-Ta stabilizes the 1WE, while, for a specific range of c_{Ta}, A_s and M_s remain higher than $100\,°$C. It is an open question whether there are other alloying elements that can prevent the formation of the ω phase without decreasing the transformation temperatures to below $100\,°$C, and this question is of great relevance for alloy design.

*alberto.ferrari@rub.de
†jutta.rogal@rub.de

In a previous study [30], we have shown that the transformation temperatures can have a nonintuitive dependence on the Ta and alloying element X concentrations c_{Ta} and c_X; the same may be true for the free energies of the β and ω phases, which determine the stability of the 1WE. Therefore, the search for new alloying elements requires experiments that cover the entire (c_{Ta}, c_X) space, and such experiments are very time-consuming if a large number of bulk samples with constant composition have to be manufactured. This naturally calls for atomistic simulations to guide the design of new Ti-Ta-X alloys.

An accurate estimate of the free energies of the α'', β, and ω phases in the (c_{Ta}, c_X) space with first-principles calculations is perhaps as inefficient as performing the corresponding experiments; a tradeoff between accuracy and efficiency can be achieved with the derivation of meaningful models that describe to a sufficiently robust approximation the transformation temperatures and the stability, and are based only on information that can be readily extracted from relatively inexpensive first-principles data (e.g., total energies, lattice parameters, densities of states, elastic constants, etc.).

In this article, we propose simple and physically motivated descriptors to predict new materials that combine a stable 1WE and transformation temperatures higher than 100 °C. By analyzing the relative stability of the α'', β, and ω phases as a function of c_{Ta} and c_X, we shortlist a set of potential candidate materials to a few promising alloys. We have been able to manufacture one of the alloys, Ti-Ta-Sc, in the composition range for which the theory predicts a stable high-temperature 1WE. In Ti-Ta-Sc, the transformation temperatures are higher than 100 °C and the ω phase is completely absent from the sample after thermal cycling, resulting in a remarkable improvement of the stability of the shape memory effect with respect to Ti-Ta, in full agreement with the predictions.

The precipitation of the ω phase presents a long-standing technological challenge in Ti-based alloys in general [38]. Over the years, and based on experience and insight, alloy constituents such as Al, Zr, O, etc., or microstructural features were associated with the suppression of ω phase formation [39–43]. Our computational design strategy may be readily applied to evaluate the relative stability of the ω phase in Ti-alloys without ad hoc or experience-based assumptions on particular alloying elements, and it may provide an important impetus toward the rational design of Ti-based alloys.

II. METHODS

A. Computational setup

The first-principles calculations have been performed using density functional theory with the plane-waves pseudopotential code VASP 5.4 [44–46]. The recommended projector augmented wave (PAW) pseudopotentials [47,48] with the PBE expression [49] for the exchange correlation functional have been employed for all the elements. The energy cutoff has been fixed to 450 eV, and the k-point meshes, distributed according to the Monkhorst-Pack scheme [50,51], have been set to $(6 \times 8 \times 8)$ and $(5 \times 5 \times 9)$ for the $3 \times 2 \times 2$ and $2 \times 2 \times 2$ supercells of the β and ω phases, respectively, and to $(8 \times 6 \times 6)$ for the orthorhombic supercells considered

in the binary interaction method [30] (see Sec. II C). The metallic electronic occupations have been smeared with the Methfessel-Paxton function [52] of order 1 with a width of 0.05 eV. Since Ti-Ta-X alloys are solid solutions, we have evaluated the relative stability of the β and ω phases using special quasirandom structures (SQS) [53], small supercells that best represent the spatial n-body correlations of random structures. The SQS were generated with a Metropolis Monte Carlo program derived from the ATAT package [54–56] taking into account the spatial correlations up to five body terms. The energy at the equilibrium volume has been computed with a Birch-Murnaghan equation-of-state fit [57,58] after complete relaxation of the atomic degrees of freedom and the cell shape. All calculations presented in this work were spin-unpolarized, as test calculations including spin-polarization for structures involving Co and Ni converged to nonmagnetic states.

B. Stability of the 1WE

Since the ω phase is observed to form from austenite, we have computed the 0 K energy difference between the β and ω phases $\Delta E^{(\beta - \omega)}(c_{Ta}, c_X)$ to describe the stability of the 1WE. If the compositional dependence of the entropy for the phase transition $\beta \rightarrow \omega$ is neglected, then $\Delta E^{(\beta - \omega)}(c_{Ta}, c_X) \leqslant 0$ signals a region in the (c_{Ta}, c_X) space where the formation of the detrimental ω phase is unfavorable.

For each potential SMA, we have fixed the composition of the alloying element X to 4 at. %, and we have calculated the Ta concentration at which $\Delta E^{(\beta - \omega)}(c_{Ta}, c_X = 4 \text{ at. \%}) = 0$. Since this concentration is also known for pure Ti-Ta [27], we have then linearly interpolated the *locus* for which $\Delta E^{(\beta - \omega)}(c_{Ta}, c_X) = 0$. This line separates the region in which ω is more stable than β from the region in which β is more stable than ω.

C. Transformation temperatures

To determine the region in the (c_{Ta}, c_X) space where the transformation temperatures are higher than 100 °C, we have calculated the 0 K energy difference between the β and α'' phases $\Delta E^{(\beta - \alpha'')}(c_{Ta}, c_X)$. In Ti-Ta based alloys, the entropy difference between the two phases depends very weakly on c_{Ta} and c_X [32] and can be assumed to be constant. Therefore, the 0 K energy difference is usually sufficient to estimate the much more computationally expensive free-energy difference between austenite and martensite.

In our previous work [30], we have shown that to a first approximation Ti-Ta-X alloys can be treated as ideal solid solutions for which $\Delta E^{(\beta - \alpha'')}$ takes the form

$$\Delta E^{\beta - \alpha''} \simeq A c_{Ta} + B c_X + C c_{Ta} c_X + D, \tag{1}$$

where A and D are parameters that depend on Ti and Ta, and B and C are parameters that depend on the interaction of the alloying element X with Ti and Ta.

To quickly estimate the coefficients B and C, we have employed the binary interaction method that we presented in Ref. [30]. According to this approach, B and C can be calculated from the energy difference between the β and α'' phases of pure Ti, pure X, and artificial binary Ti-X and Ta-X solid solutions.

In fact, the mixing energy of a system with elements of species n (n = Ti, Ta, X) in the phase (i), defined as

$$^{\mathrm{mix}}E^{(\mathrm{i})} := E^{(\mathrm{i})} - \sum_n c_n E_n^{(\mathrm{i})}, \qquad (2)$$

can be expanded as [30]

$$^{\mathrm{mix}}E^{(\mathrm{i})} = \sum_{n,m} k_{nm}^{(\mathrm{i})} c_n c_m + O[c^3] \qquad (3)$$

for regular solid solutions. As detailed in Ref. [30], the quadratic coefficients $k_{nm}^{(\mathrm{i})}$ of this expansion for the β and α'' phases can be fitted from the mixing energies of binary n-m solid solutions. If the difference between these quadratic coefficients is expressed as

$$\Delta k_{nm} := k_{nm}^{(\beta)} - k_{nm}^{(\alpha'')} \qquad (4)$$

and furthermore

$$\lambda_n := E_n^{(\beta)} - E_n^{(\alpha'')}, \qquad (5)$$

then the coefficients B and C are simply given by [30]

$$\begin{aligned} B &= \Delta k_{\mathrm{Ti}X} + \lambda_X - \lambda_{\mathrm{Ti}}, \\ C &= \Delta k_{\mathrm{Ta}X} - \Delta k_{\mathrm{Ti}X}. \end{aligned} \qquad (6)$$

With the binary interaction method, it is possible to calculate the energy difference $\Delta E^{\beta - \alpha''}$ in the entire composition range using Eq. (1). This considerably reduces the computational cost associated with the estimation of the transformation temperatures in the (c_{Ta}, c_X) space.

The approximations underlying this approach derive from the truncation of the expansion in Eq. (3) and from the fitting of the coefficients $k_{nm}^{(\mathrm{i})}$, which can be biased by the fact that not every pair of elements n-m can form solid solutions in a specific phase (i). Furthermore, the validity of Eq. (6) is limited to small c_X, as mentioned in Ref. [30].

D. Experimental setup

The Ti-Ta-Sc sample has been prepared by arc-melting high-purity Ti, Ta, and Sc raw materials. The SMA ingot has been remelted 15 times to achieve chemical homogeneity. The actual composition of the ingot has been measured by energy-dispersive x-ray analysis (EDX) in a scanning electron microscope and determined as approximately $\mathrm{Ti_{66.2}Ta_{31.5}Sc_{2.3}}$. Details on the thermomechanical processing and the chemical analysis are given in Refs. [13,59].

The fully recrystallized alloy has been subjected to thermal cycling in a differential scanning calorimetry instrument of type TA 2920 CE. Details on DSC operating parameters are given in Refs. [13,35].

To obtain electron-transparent samples for the TEM microstructure analysis, a focused ion-beam system of the type FEI Helios G4 CX DualBeam has been used. The TEM characterization has been conducted on a Tecnai F20 G2 Supertwin FEG TEM, operating at an acceleration voltage of 200 kV. All further details on TEM sample preparation and analysis are available in Refs. [25,35,59,60].

III. RESULTS AND DISCUSSION

We have restricted our search for possible alloying elements to transition metals and p-valent metals. From these candidates we have excluded noble gases, noble metals, poisonous or radioactive elements, and the $2p$ elements, which are more likely to occupy interstitial sites rather than producing substitutional defects. Some of the remaining elements, namely Al, V, Cr, Fe, Zr, Mo, Sn, and Hf, have already been investigated by Buenconsejo *et al.* [21], albeit at a fixed Ta concentration. We have chosen to study eight new elements—Si, Sc, Co, Ni, Cu, In, Sb, and Bi—as possible candidates for alloying elements in new SMAs. To benchmark our approach, we have chosen to analyze also Ti-Ta-Al, for which detailed experimental results are already present in the literature [22,30].

For each alloying element, we have investigated the site preference of the substitutional defects in both the β and ω phases. An example of the formation energies of these two phases, defined as

$$E_f^{(\mathrm{i})} = E^{(\mathrm{i})} - c_{\mathrm{Ti}}E_{\mathrm{Ti}} - c_{\mathrm{Ta}}E_{\mathrm{Ta}} - c_X E_X, \qquad (7)$$

where $E^{(\mathrm{i})}$ is the total energy of Ti-Ta-X in phase (i) (β or ω), E_{Ti} is the energy of hcp Ti, E_{Ta} is the energy of bcc Ta, and E_X is the energy of the most stable structure of the element X, is displayed in Fig. 1 for Ti-17Ta-4Al (with 17 at. % Ta and 4 at. % Al). The x-axis corresponds to the number of Ta atoms in the first-nearest-neighbor shell of Al. For β, the formation energy increases with an increasing number of Ta nearest neighbors for all the investigated alloys, as already noted for Ti-Ta-Al, Ti-Ta-Sn, and Ti-Ta-Zr [30], apart from Ti-Ta-Sc, for which it is approximately constant. For ω, the formation energy is instead independent of the number of Ta nearest neighbors, but it depends on the Wyckoff site in which the alloying element is positioned: ω is characterized
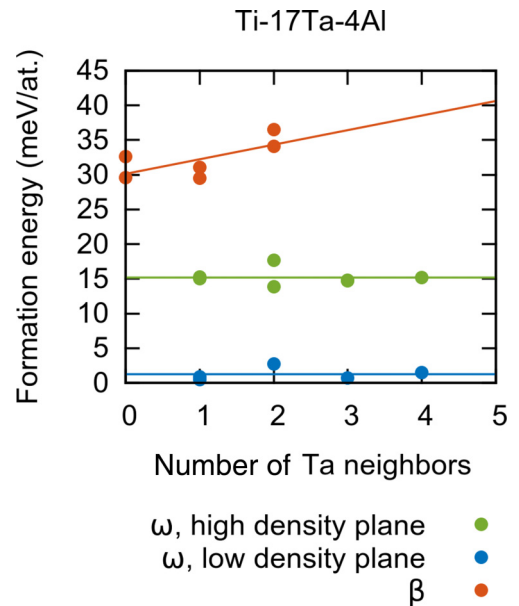

FIG. 1. Formation energy of Ti-17Ta-4Al in the β and ω phases. For the ω phase, the formation energy is different if Al occupies the Wyckoff position in the high- or in the low-density plane.
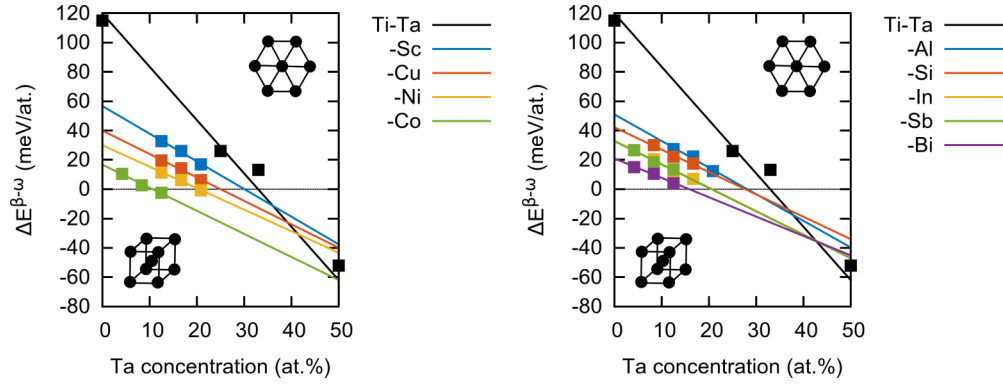
FIG. 2. Energy difference between β and ω as a function of Ta concentration for Ti-Ta-4X alloys, where X is a d-valent (left) or p-valent (right) element.

by three sites, two of which are equivalent to each other and are located on a high-density plane perpendicular to the [0001] direction, while the other one is located on a low-density plane perpendicular to the same direction. The elements with an atomic radius larger than Ti (Al, Sc, In, Sb, and Bi) show a site preference for the low-density plane, whereas the elements with an atomic radius smaller than Ti (Si, Co, Ni, and Cu) show a site preference for the high-density plane.

Although DFT calculations show ordering effects at low temperature [30], during the martensitic transformation the alloying elements are trapped in their local environment, and a fully disordered, metastable phase is retained even at low temperature. Therefore, we have occupied the lattice sites of all the phases stochastically. We have assumed $8 \times c_{\text{Ta}}$ as the number of Ta nearest neighbors in β (8 is the number of first nearest neighbors in a bcc structure) and computed the corresponding formation energy. For the formation energy of ω we have averaged the formation energies of configurations with substitutions in the three Wyckoff positions.

Figure 2 shows the resulting energy difference $\Delta E^{(\beta-\omega)}$ as a function of c_{Ta} with fixed $c_X = 4$ at. % for the d (left) and p (right) valent alloying elements. For comparison, the data for pure Ti-Ta taken from Chakraborty *et al.* [27] are also reported (black dots). A negative value of $\Delta E^{(\beta-\omega)}$ indicates a stable 1WE, and the intercept with the x-axis indicates the concentration at which the energies of β and ω are equal for $c_X = 4$ at. %.

It can be seen that all selected alloying elements destabilize the detrimental ω phase with respect to β. Among the p-valent elements there is a clear trend with the size of the alloying element: elements with higher atomic radii tend to destabilize the ω phase more. This can be understood from the fact that configurations with relatively large elements in the high-density plane of the ω phase are energetically very unfavorable. No clear trend in terms of size or band filling is instead recognized for the d-valent elements.

To evaluate the compositional dependence of the transformation temperatures as described by Eq. (1), we have taken the values of $A = -23.9$ K/at. % and $D = 1140$ K from our previous work [30]. To estimate the coefficients B and C, we have fitted the mixing energy of binary Ti-X and Ta-X alloys using Eq. (2) as described in Ref. [30].

A. Benchmark: Ti-Ta-Al

The predictions of our model for the stability and high-temperature regions in Ti-Ta-Al are reported in Fig. 3. The color scale indicates the predicted M_s as a function of c_{Ta} and c_X from Eq. (1). The solid red line separates the predicted regions of high (left) and low (right) M_s, and the blue line separates the predicted regions where ω is stable (left) and unstable (right). A region of the $(c_{\text{Ta}}, c_{\text{Al}})$ plane delimited with a blue line on the left and a red line on the right is predicted to be characterized by $M_s > 100\,^{\circ}\text{C}$ *and* a stable 1WE. From Fig. 3 it can be deduced that such a region cannot be obtained in binary Ti-Ta, but only with the addition of Al, in agreement with previous investigations [21,22,25].

The experimental curves [22] for the stability (blue) and high-temperature (red) regions are displayed as dashed lines in Fig. 3 for comparison. The stability line from our model agrees well with the experimental measurements, and the stability/instability regions can be predicted within roughly
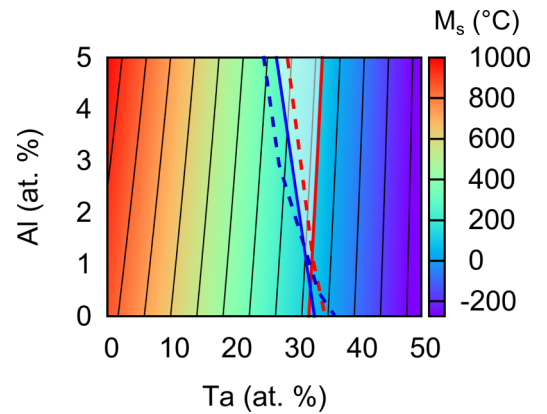

FIG. 3. Martensitic start temperature predicted by the theoretical model as a function of the Ta and Al concentration in Ti-Ta-Al. The red line divides the region in which $M_s > 100\,^{\circ}\text{C}$ (left) from the region in which $M_s < 100\,^{\circ}\text{C}$ (right). The blue line separates the region in which the ω phase is stable (left) from the region in which the ω phase is unstable (right). The shaded area between the blue and red lines is a region where the 1WE is stable and has $M_s > 100\,^{\circ}\text{C}$. Solid lines are predictions from our model, and dashed lines are experimental data from Ref. [22].

3 at. % Ta. The red line from our model has a positive slope, indicating that for increasing Al content M_s would increase slightly at $c_{Ta} \sim 30$ at. %. As already pointed out in our previous work [30], this is not in quantitative agreement with experiment, as in Ti-Ta-Al the transformation temperatures have been observed to increase for increasing c_{Al} only for $c_{Ta} < 16$ at. % [30]. This is due to the approximations within the binary interaction model. Despite this, our model is able to predict qualitatively the existence of a region with high temperature and stable 1WE and is thus suitable to guide the assessment of new alloys.

B. New candidate alloys

Figure 4 shows the predicted diagrams for the stability and martensitic start temperature for Ti-Ta-Si, Ti-Ta-Ni, Ti-Ta-Cu, Ti-Ta-Co, Ti-Ta-Sb, Ti-Ta-Bi, Ti-Ta-In, and Ti-Ta-Sc. In general, the elements that destabilize the ω phase the most, such as Co and Bi, are found to lower M_s considerably,

because the β phase is strongly stabilized. For most of the elements, a balance between stability and high transformation temperatures can be found by an appropriate tuning of c_{Ta} and c_X, although some alloys appear to be more promising than others.

In particular, for Ti-Ta-Si we predict no region of stability and high-transformation temperature, thus this alloy is unlikely to be a good SMA. The additions of Ni and Cu result in very narrow regions of stability and high transformation temperature, with a width comparable to the error bars of our model. A definitive conclusion concerning the performance of Ti-Ta-Ni and Ti-Ta-Cu as SMAs is thus not possible. Alloying Co is predicted to decrease M_s substantially, although a region of stability and high transformation temperature can be identified at relatively low c_{Ta}. However, the stability at such a low c_{Ta} may still be compromised by the precipitation of athermal ω particles with a Ti-rich composition [31]; therefore, we presume that Co may not improve the stability of the 1WE.

The p-valent elements Sb, Bi, and In, characterized by a similar chemistry upon alloying to Ti-Ta, might be potential candidates to stabilize the 1WE, although they are predicted to decrease M_s at all c_{Ta}. In particular In, in the same period as Sn and isoelectronic to Al, shares the same beneficial properties of these two elements, already known to favor the stability of the 1WE [21].

Finally, the alloy Ti-Ta-Sc seems to be superior to the other investigated potential SMAs because the addition of Sc can destabilize the ω phase while keeping M_s high even at $c_{Ta} \sim 30$ at. %. Our calculations predict that M_s should increase slightly with increasing c_{Sc}. An increase of the energy difference between β and α'' has been observed recently also in Ti-Nb-Sc [61] and can be imputed to a band-filling effect: alloying Sc decreases the number of d valence electrons of the alloy and destabilizes the β phase. This decrease of the d-electron count, however, does not result in a stabilization of the ω phase but in a destabilization, presumably because of the size mismatch between Ti and Sc: Alloying Sc, with an atomic radius bigger than that of Ti, is not favorable in the ω phase. Given the very promising results for this alloy, we decided to investigate the Ti-Ta-Sc system experimentally.

C. Experimental validation for Ti-Ta-Sc

To validate the theoretical predictions, we have fabricated a Ti-Ta-Sc alloy with $c_{Ta} = 31.5$ at. % and $c_{Sc} = 2.3$ at. %, a composition inside the proposed high-temperature and stability region for this alloy, and we have evaluated the functional and microstructural stability of this alloy with differential scanning calorimetry (DSC) and transmission electron microscopy (TEM).

Figure 5 compares the DSC data obtained from thermal cycling experiments on Ti-Ta and Ti-Ta-Sc. The exothermic peaks on cooling (positive heat flow) indicate the formation of martensite, whereas the endothermic peaks on heating (negative heat flow) are associated with the reverse transformation $\alpha'' \rightarrow \beta$. Both alloys have been subjected to cyclic heating and cooling, and the cycle numbers are marked with c_i.

As indicated by the strong shift of the transformation peaks to lower temperatures in Fig. 5(a), the phase transformation in binary Ti-Ta alloy is not stable and degrades within only five
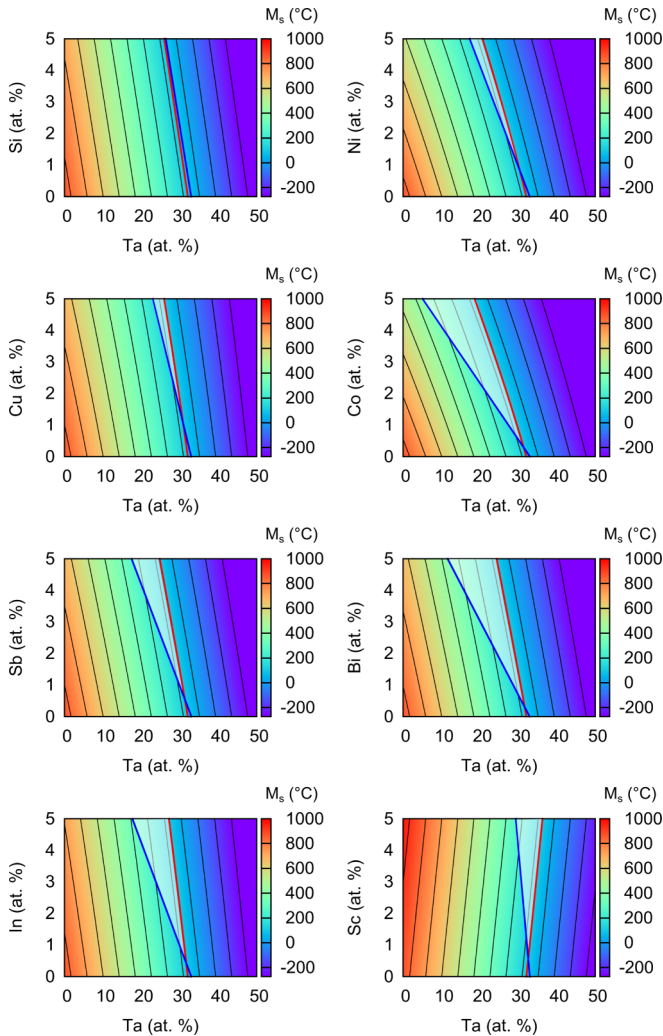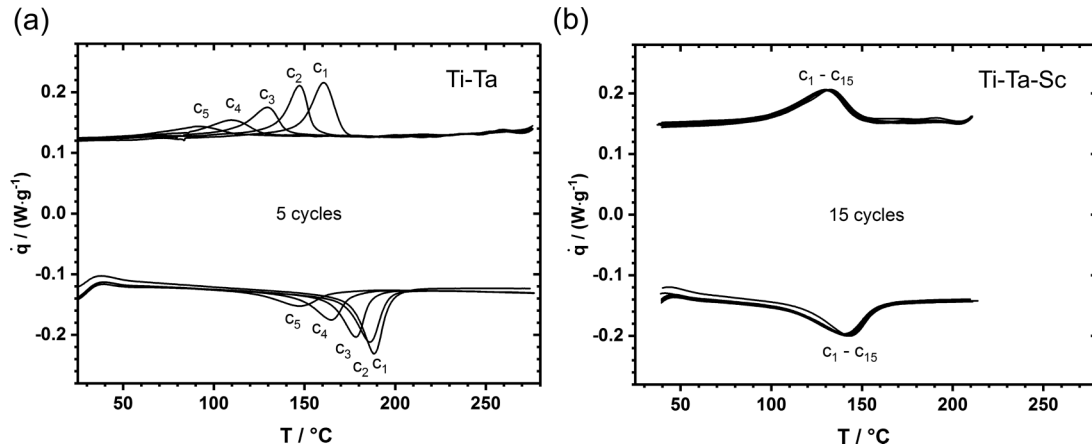

FIG. 4. Predicted martensitic starting temperature as a function of composition for (left to right, top to bottom): Ti-Ta-Si, Ti-Ta-Ni, Ti-Ta-Cu, Ti-Ta-Co, Ti-Ta-Sb, Ti-Ta-Bi, Ti-Ta-In, and Ti-Ta-Sc. The red and blue lines mark the region of high transformation temperature and high stability, respectively, as detailed in Fig. 3.

FIG. 5. (a) DSC data for five heating/cooling cycles of binary Ti-Ta with $c_{Ta} = 30$ at. %, where a rapid degradation can be observed. (b) 15 DSC cycles of Ti-Ta-Sc with $c_{Ta} = 31.5$ at. % and $c_{Sc} = 2.3$ at. %, which exhibits a remarkably stable behavior and transformation temperatures higher than $100\,^{\circ}$C. A comparison of the data in (a) and (b) provides clear evidence for the improved functional stability of Ti-Ta-Sc over Ti-Ta.

cycles. For the unstable binary alloy, thermal cycling is also associated with a change in the latent heat, which corresponds to the area below the DSC peaks. The small transformation peaks obtained in the fifth cycle of Ti-Ta suggest that a significantly smaller volume fraction of the material undergoes a martensitic and reverse transformation during cycling.

In contrast, the situation is drastically different in Fig. 5(b) for the new Ti-Ta-Sc alloy. Ti-Ta-Sc shows a very stable transformation behavior, as all heating/cooling curves coincide almost perfectly up to at least 15 cycles. Furthermore, the martensitic and reverse transformations are observed at a temperature higher than $100\,^{\circ}$C, in agreement with the theoretical predictions.

The microstructures of Ti-Ta and Ti-Ta-Sc after thermal cycling have also been characterized by TEM to identify potential degradation mechanisms. For binary Ti-Ta, a selected area diffraction pattern at the $[101]_{\beta}$ zone axis, shown in Fig. 6(a), reveals strong diffraction intensities at $1/3 \langle 211 \rangle_{\beta}$ positions, associated with the presence of the ω phase. Based on the dark field image in Fig. 6(b), obtained for the marked ω reflection, nanoscaled ω precipitates with a high volume fraction have been identified in Ti-Ta.

Conversely, the selected area diffraction pattern of the Ti-Ta-Sc sample at the $[001]_{\alpha''}$ zone axis in Fig. 6(c) indicates a purely martensitic matrix, and no diffraction intensity corresponding to the ω phase at $1/3 \langle 211 \rangle_{\beta}$ positions is observed. Therefore, in agreement with the theoretical predictions, no traces of ω phase precipitation are detected. Accordingly, the dark field image in Fig. 6(d) obtained for the encircled $[\bar{1}10]$ reflection shows a microstructure with typical martensitic features. This proves that the addition of Sc to Ti-Ta results in a complete suppression of the detrimental ω phase.

IV. CONCLUSIONS

We presented a theory-guided alloy optimization of Ti-Ta-*X* SMAs that can discover alloy compositions demonstrating a superior stability with respect to thermal cycling and high transformation temperatures. Our first-principles

screening, based on 0 K energy differences between random structures, has identified at least four potential stable and high-temperature SMAs, namely Ti-Ta-Sb, Ti-Ta-Bi, Ti-Ta-In, and Ti-Ta-Sc. We have experimentally fabricated the most promising of these new alloys, Ti-Ta-Sc, and we have observed an extremely good stability of the 1WE because of the
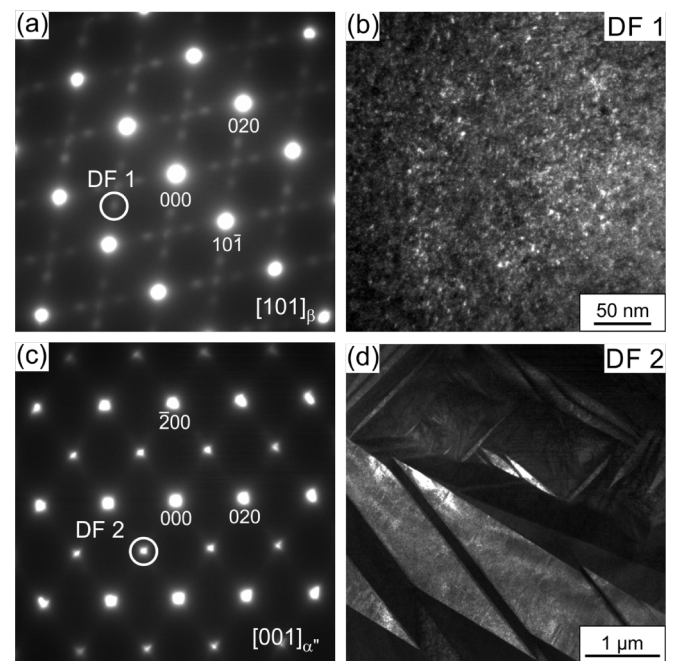

FIG. 6. TEM analysis of the Ti-Ta and Ti-Ta-Sc samples after thermal cycling. (a) Selected-area diffraction pattern of the binary Ti-Ta sample at the $[101]_{\beta}$ zone axis, revealing diffraction intensities of the ω phase. (b) Dark-field (DF) image taken for the reflection marked DF1 in (a), indicating the presence of nanoscaled ω precipitates. (c) Selected-area diffraction pattern at the $[001]_{\alpha''}$ zone axis of the Ti-Ta-Sc sample, showing no ω reflections. (d) Only martensitic features are identified in the DF image obtained for the α'' diffraction intensity marked DF2 in (c).

full suppression of the ω phase, and transformation temperatures higher than $100\,^\circ$C, in agreement with the predictions of the model. The ternary alloys described in this study may open new opportunities for the application of SMAs in high-temperature environments; these opportunities may be even broader due to the possibility of applying the workflow described here to explore other ternary Ti-Ta-*X* alloys. Our approach is fully transferable to other, even quaternary or multicomponent Ti-alloys, and it forms the basis for a rational design of ω-free alloys.

[1] A. Ölander, The crystal structure of AuCd, Z. Kristall. **83**, 145 (1932).

[2] L. C. Chang and T. A. Read, Plastic deformation and diffusionless phase changes in metals - The gold-cadmium beta phase, JOM **3**, 47 (1951).

[3] H. Funakubo, *Shape Memory Alloys* (Gordon and Breach, London, 1987).

[4] K. Otsuka and C. M. Waymann, *Shape Memory Materials* (Cambridge University Press, Cambridge, 1998).

[5] T. W. Duerig, K. N. Melton, D. Stckel, and C. M. Wayman, *Engineering Aspects of Shape Memory Alloys* (Butterworth-Heinemann, London, 1990).

[6] E. Hornbogen, in *Shape Memory Alloys*, edited by W. G. J. Bunk, Advanced structural and functional materials (Springer-Verlag, Berlin, 1991).

[7] K. Otsuka and X. Ren, Recent developments in the research of shape memory alloys, Intermetallics **7**, 511 (1999).

[8] J. Van Humbeeck, Shape memory alloys: A material and a technology, Adv. Eng. Mater. **3**, 837 (2001).

[9] P. K. Kumar and D. C. Lagoudas, *Introduction to Shape Memory Alloys* (Springer, Boston, 2008).

[10] W. J. Buehler, J. V. Gilfrich, and R. C. Wiley, Effect of low temperature phase changes on the mechanical properties of alloys near composition TiNi, J. Appl. Phys. **34**, 1475 (1963).

[11] K. Otsuka and X. Ren, Physical metallurgy of Ti-Ni-based shape memory alloys, Prog. Mater. Sci. **50**, 511 (2005).

[12] J. Frenzel, E. P. George, A. Dlouhý, C. Somsen, M. F. X. Wagner, and G. Eggeler, Influence of Ni on martensitic phase transformations in NiTi shape memory alloys, Acta Mater. **58**, 3444 (2010).

[13] J. Frenzel, A. Wieczorek, I. Opahle, B. Maass, R. Drautz, and G. Eggeler, On the effect of alloy composition on martensite start temperatures and latent heats in Ni-Ti-based shape memory alloys, Acta Mater. **90**, 213 (2015).

[14] G. S. Firstov, J. Van Humbeeck, and Y. N. Koval, High-temperature shape memory alloys: Some recent developments, Mat. Sci. Eng. A **378**, 2 (2004).

[15] J. Ma, I. Karaman, and R. D. Noebe, High temperature shape memory alloys, Int. Mater. Rev. **55**, 257 (2010).

[16] Y. A. Bagarjatskii, G. I. Nosova, and T. V. Tagunova, Laws of formation of metastable phase in titanium alloys, Dokl. Akad. Nauk SSSR **122**, 593 (1958).

[17] K. A. Bywater and J. W. Christian, Martensitic transformations in titanium-tantalum alloys, Philos. Mag. **25**, 1249 (1972).

[18] S. G. Fedotov, T. V. Chelidze, Y. K. Kovneristyj, and V. V. Sanadze, Phase structure, critical points M_s and A_s of martensitic transformation and elastic properties of metastable alloys of the Ti-Ta system, Fiz. Met. Metalloved. **60**, 567 (1985).

[19] S. G. Fedotov, T. V. Chelidze, Y. K. Kovneristyj, and V. V. Sanadze, Phase-transformation in metastable alloys of the Ti-Ta system during heating, Fiz. Met. Metalloved. **62**, 328 (1986).

[20] P. J. S. Buenconsejo, H. Y. Kim, H. Hosoda, and S. Miyazaki, Shape memory behavior of Ti-Ta and its potential as a high-temperature shape memory alloy, Acta Mater. **57**, 1068 (2009).

[21] P. J. S. Buenconsejo, H. Y. Kim, and S. Miyazaki, Effect of ternary alloying elements on the shape memory behavior of Ti-Ta alloys, Acta Mater. **57**, 2509 (2009).

[22] P. J. S. Buenconsejo, H. Y. Kim, and S. Miyazaki, Novel β-TiTaAl alloys with excellent cold workability and a stable high-temperature shape memory effect, Scr. Mater. **64**, 1114 (2011).

[23] H. Y. Kim, T. Fukushima, P. J. S. Buenconsejo, T. H. Nam, and S. Miyazaki, Martensitic transformation and shape memory properties of Ti-Ta-Sn high temperature shape memory alloys, Mater. Sci. Eng. A **528**, 7238 (2011).

[24] T. Niendorf, P. Krooß, E. Batyrsina, A. Paulsen, J. Frenzel, G. Eggeler, and H. J. Maier, On the functional degradation of binary titanium-tantalum high-temperature shape memory alloys—a new concept for fatigue life extension, Funct. Mater. Lett. **7**, 1450042 (2014).

[25] T. Niendorf, P. Krooß, E. Batyrsina, A. Paulsen, Y. Motemani, A. Ludwig, P. Buenconsejo, J. Frenzel, G. Eggeler, and H. J. Maier, Functional and structural fatigue of titanium tantalum high temperature shape memory alloys (HT SMAs), Mater. Sci. Eng. A **620**, 359 (2015).

[26] T. Niendorf, P. Krooß, C. Somsen, R. Rynko, A. Paulsen, E. Batyrsina, J. Frenzel, G. Eggeler, and H. J. Maier, Cyclic degradation of titanium-tantalum high-temperature shape memory alloys: The role of dislocation activity and chemical decomposition, Funct. Mater. Lett. **8**, 1550062 (2015).

[27] T. Chakraborty, J. Rogal, and R. Drautz, Martensitic transformation between competing phases in Ti-Ta alloys: A solid-state nudged elastic band study, J. Phys.: Condens. Matter **27**, 115401 (2015).

[28] T. Chakraborty, J. Rogal, and R. Drautz, Unraveling the composition dependence of the martensitic transformation temperature: A first-principles study of Ti-Ta alloys, Phys. Rev. B **94**, 224104 (2016).

[29] P. M. Kadletz, Y. Motemani, J. Iannotta, S. Salomon, C. Khare, L. Grossmann, H. J. Maier, A. Ludwig, and W. W. Schmahl,

Crystallographic structure analysis of a Ti-Ta thin film materials library fabricated by combinatorial magnetron sputtering, ACS Comb. Sci. **20**, 137 (2018).

[30] A. Ferrari, A. Paulsen, J. Frenzel, J. Rogal, G. Eggeler, and R. Drautz, Unusual composition dependence of transformation temperatures in Ti-Ta-X shape memory alloys, Phys. Rev. Mater. **2**, 073609 (2018).

[31] A. Ferrari, P. Kadletz, T. Chakraborty, K. Liao, D. Langenkämper, Y. Motemani, A. Paulsen, Y. Lysogorskiy, J. Frenzel, J. Rogal, A. Ludwig, C. Somsen, R. Drautz, and W. W. Schmahl, Reconciling experimental and theoretical data in the structural analysis of Ti-Ta shape memory alloys, Shap. Mem. Superelast. **5**, 6 (2019).

[32] A. Ferrari, D. G. Sangiovanni, J. Rogal, and R. Drautz, First-principles characterization of reversible martensitic transformations, Phys. Rev. B **99**, 094107 (2019).

[33] H. Y. Kim and S. Miyazaki, *Ni-free Ti-based Shape Memory Alloys* (Butterworth-Heinemann, Oxford, 2018).

[34] H. J. Maier, E. Karsten, A. Paulsen, D. Langenkämper, P. Decker, J. Frenzel, C. Somsen, A. Ludwig, G. Eggeler, and T. Niendorf, Microstructural evolution and functional fatigue of a Ti-25Ta high-temperature shape memory alloy, J. Mater. Res. **32**, 4287 (2017).

[35] A. Paulsen, J. Frenzel, D. Langenkämper, R. Rynko, P. Kadletz, L. Grossmann, W. W. Schmahl, C. Somsen, and G. Eggeler, A kinetic study on the evolution of martensitic transformation behavior and microstructures in Ti-Ta high-temperature shape-memory alloys during aging, Shap. Mem. Superelasticity **5**, 16 (2019).

[36] J. L. Murray, The Ta-Ti (tantalum-titanium) system, Bull. Alloy Phase Diagr. **2**, 62 (1981).

[37] X. H. Zheng, J. H. Sui, X. Zhang, Z. Y. Yang, H. B. Wang, X. H. Tian, and W. Cai, Thermal stability and high-temperature shape memory effect of Ti-Ta-Zr alloy, Scr. Mater. **68**, 1008 (2013).

[38] B. S. Hickman, The formation of omega phase in titanium and zirconium alloys: A review, J. Mater. Sci. **4**, 554 (1969).

[39] J. I. Qazi, B. Marquardt, L. F. Allard, and H. J. Rack, Phase transformations in Ti-35Nb-7Zr-5Ta-(0.06–0.68)O alloys, Mater. Sci. Eng. C **25**, 389 (2005).

[40] R. J. Talling, R. J. Dashwood, M. Jackson, and D. Dye, On the mechanism of superelasticity in gum metal, Acta Mater. **57**, 1188 (2009).

[41] S. Guo, Q. Meng, L. Hu, G. Liao, X. Zhao, and H. Xu, Suppression of isothermal ω phase by dislocation tangles and grain boundaries in metastable β-type titanium alloys, J. Alloys Compd. **550**, 35 (2013).

[42] E. L. Pang, E. J. Pickering, S. I. Baik, D. N. Seidman, and N. G. Jones, The effect of zirconium on the omega phase in Ti-24Nb-[0–8]Zr (at.%) alloys, Acta Mater. **153**, 62 (2018).

[43] M. Tane, H. Nishiyama, A. Umeda, N. L. Okamoto, K. Inoue, M. Luckabauer, Y. Nagai, T. Sekino, T. Nakano, and T. Ichitsubo, Diffusionless isothermal omega transformation in

titanium alloys driven by quenched-in compositional fluctuations, Phys. Rev. Mater. **3**, 043604 (2019).

[44] G. Kresse and J. Hafner, *Ab initio* molecular dynamics for liquid metals, Phys. Rev. B **47**, 558 (1993).

[45] G. Kresse and J. Furthmüller, Efficiency of *ab-initio* total energy calculations for metals and semiconductors using a plane-wave basis set, Comput. Mat. Sci. **6**, 15 (1996).

[46] G. Kresse and J. Furthmüller, Efficient iterative schemes for *ab initio* total-energy calculations using a plane-wave basis set, Phys. Rev. B **54**, 11169 (1996).

[47] P. E. Blöchl, Projector augmented-wave method, Phys. Rev. B **50**, 17953 (1994).

[48] G. Kresse and D. Joubert, From ultrasoft pseudopotentials to the projector augmented-wave method, Phys. Rev. B **59**, 1758 (1999).

[49] J. P. Perdew, K. Burke, and M. Ernzerhof, Generalized Gradient Approximation Made Simple, Phys. Rev. Lett. **77**, 3865 (1996).

[50] A. Baldereschi, Mean-value point in the Brillouin zone, Phys. Rev. B **7**, 5212 (1973).

[51] H. J. Monkhorst and J. D. Pack, Special points for Brillouin-zone integrations, Phys. Rev. B **13**, 5188 (1976).

[52] M. P. A. T. Methfessel and A. T. Paxton, High-precision sampling for Brillouin-zone integration in metals, Phys. Rev. B **40**, 3616 (1989).

[53] A. Zunger, S. H. Wei, L. G. Ferreira, and J. E. Bernard, Special Quasirandom Structures, Phys. Rev. Lett. **65**, 353 (1990).

[54] J. von Pezold, A. Dick, M. Friák, and J. Neugebauer, Generation and performance of special quasirandom structures for studying the elastic properties of random alloys: Application to Al-Ti, Phys. Rev. B **81**, 094203 (2010).

[55] J. Koßmann, T. Hammerschmidt, S. Maisel, S. Müller, and R. Drautz, Solubility and ordering of Ti, Ta, Mo and W on the Al sublattice in L1$_2$-Co$_3$Al, Intermetallics **64**, 44 (2015).

[56] A. van de Walle, M. Asta, and G. Ceder, The alloy theoretic automated toolkit: A user guide, Calphad **26**, 539 (2002).

[57] F. D. Murnaghan, The compressibility of media under extreme pressures, Proc. Natl. Acad. Sci. USA **30**, 244 (1944).

[58] F. Birch, Finite elastic strain of cubic crystals, Phys. Rev. **71**, 809 (1947).

[59] J. Zhang, R. Rynko, J. Frenzel, C. Somsen, and G. Eggeler, Ingot metallurgy and microstructural characterization of Ti-Ta alloys, Int. J. Mater. Res. **105**, 156 (2014).

[60] D. Langenkämper, A. Paulsen, C. Somsen, J. Frenzel, and G. Eggeler, On the oxidation behavior and its influence on the martensitic transformation of Ti-Ta high-temperature shape memory alloys, Shap. Mem. Superelasticity **5**, 63 (2019).

[61] D. Minami, T. Uesugi, Y. Takigawa, and K. Higashi, First-principles study of transformation strains and phase stabilities in α'' and β Ti-Nb-X alloys, J. Alloys Compd. **716**, 37 (2017).

[62] http://www.for1766.de.